

# Journal of Materials Chemistry A

Accepted Manuscript



This is an *Accepted Manuscript*, which has been through the Royal Society of Chemistry peer review process and has been accepted for publication.

*Accepted Manuscripts* are published online shortly after acceptance, before technical editing, formatting and proof reading. Using this free service, authors can make their results available to the community, in citable form, before we publish the edited article. We will replace this *Accepted Manuscript* with the edited and formatted *Advance Article* as soon as it is available.

You can find more information about *Accepted Manuscripts* in the [Information for Authors](#).

Please note that technical editing may introduce minor changes to the text and/or graphics, which may alter content. The journal's standard [Terms & Conditions](#) and the [Ethical guidelines](#) still apply. In no event shall the Royal Society of Chemistry be held responsible for any errors or omissions in this *Accepted Manuscript* or any consequences arising from the use of any information it contains.

Cite this: DOI: 10.1039/c0xx00000x

www.rsc.org/xxxxxx

ARTICLE TYPE

# From Semiconductors to Semimetals: Bismuth as Photocatalyst for NO Oxidation in Air

Qian Zhang,<sup>a,b</sup> Ying Zhou,\*<sup>a,b</sup> Fang Wang,<sup>b</sup> Fan Dong,<sup>c</sup> Wei Li,<sup>b</sup> Haimin Li<sup>b</sup> and Greta R. Patzke<sup>d</sup>*Received (in XXX, XXX) Xth XXXXXXXXXX 20XX, Accepted Xth XXXXXXXXXX 20XX*

DOI: 10.1039/b000000x

Elemental photocatalysts have recently been proposed as an interesting materials type for alternatives to conventional semiconductor compounds. In this study, we demonstrate that not only elements with semiconducting properties are photocatalytically active by introducing semimetallic bismuth for the photooxidation of NO. Black Bi films were prepared via an electrochemical deposition approach. Both density functional theory (DFT) calculations and temperature dependence electrical resistivity measurements pointed out that the obtained films exhibited semimetallic behavior. The Bi films were easily oxidized upon exposure to air. However, electrochemical reduction of the surface amorphous oxide layer led to a more than 4-fold enhancement of the photocurrent density of the Bi films. The detection of hydroxyl radicals with electron spin resonance (ESR) investigations further confirmed the photogeneration of electrons and holes. A 37.7% removal ratio of NO over Bi films was observed under UV light irradiation with no significant reduction of photocatalytic activity after five cycles. Given that the conduction and valence bands of semimetallic Bi overlap, the associated excitation processes are more complex in comparison with semiconductor photocatalysts, thereby indicating a different photocatalytic mechanism. The present study points out new directions for developing semimetallic photocatalysts.

## 1. Introduction

As a potential solution to the global energy crisis and environmental pollution, photocatalytic solar-energy conversion has been attracting worldwide attention.<sup>1</sup> TiO<sub>2</sub> is by far the most widely used and investigated photocatalyst due to its high efficiency and photostability.<sup>2</sup> Along these lines, hundreds of compounds have been explored as potential photocatalysts including oxides, sulfides, nitrides and phosphates, such as Ag<sub>3</sub>PO<sub>4</sub> with very promising photooxidation properties<sup>3a</sup> or Cu<sub>2</sub>(OH)PO<sub>4</sub> exhibiting photocatalytic activity in the near infrared range.<sup>3b</sup> Concerning unconventional photocatalytic materials, C<sub>3</sub>N<sub>4</sub> can generate H<sub>2</sub> from water even in the absence of noble metals.<sup>4</sup> In addition to the large number of complex photocatalytically active compounds, most recently much simpler materials (Si, P, S, B) were identified as promising candidates for targeted photocatalysis reactions due to their suitable band structure.<sup>5</sup> From the materials design point of view, photocatalytic systems based on primary elements offer more elegant and direct tuning options than more complex compounds. Therefore, elemental photocatalysts open up new avenues for discovery of hitherto unknown types of catalytic materials.<sup>6</sup> To date, the reported elemental photocatalysts are mainly semiconductors which have been exclusively investigated with respect to photocatalytic applications. Generally, light absorption across the band gap between the valence and conduction bands in semiconductors generates electron-hole pairs which subsequently migrate to the semiconductor surface to participate in redox reactions, in close analogy to electrolysis processes.<sup>1a</sup> On the other hand, metals differ from semiconductors through the absence of an energy gap separating occupied and unoccupied

levels, so that they are rarely used as photocatalysts due to the resulting very fast recombination of photocarriers. Nevertheless, the application potential of metallic materials as a new and unconventional class of photocatalysts is just about to be discovered. The work of Irvine et al., for example, clearly demonstrated that metallic perovskite oxides facilitate kinetic charge separation which is effective in decomposing of methylene blue, as well as in photocatalytic hydrogen and oxygen evolution from water splitting.<sup>7</sup> This discovery provides a new perspective for photocatalyst screening and thus motivated us to search for novel elemental photocatalysts with metallic properties.

Bismuth, in bulk form, is a semimetal with unusual electronic properties resulting from its small electron effective mass, large mean free path and low charge carrier density.<sup>8</sup> Consequently, bismuth has been widely used as a model system to study quantum transport and finite size effects.<sup>9</sup> Induction of a semimetal-semiconductor transition is possible through reduction of the crystallite size below a critical value.<sup>10</sup> Moreover, Bi (III)-based oxides, such as BiVO<sub>4</sub>, Bi<sub>2</sub>WO<sub>6</sub> and Bi<sub>2</sub>MoO<sub>6</sub>, have attracted considerable attention as visible light driven photocatalysts due to the hybridized valence band (VB) formed by the Bi 6s and O 2p levels which can narrow the band gap and enhance the mobility of photogenerated holes in the VB.<sup>11</sup> Despite manifold studies on bismuth based oxides, the possibility of using elemental bismuth as a photocatalyst in its own right has rarely been considered<sup>12</sup> and especially, the photocatalytic mechanisms for semimetallic bismuth have never been explored to the best of our knowledge.

Herein, we report a facile electrochemical deposition approach to prepare black bismuth films at room temperature. To the best of our knowledge, this is the first example of an elemental

photocatalyst with semimetallic properties. Density functional theory (DFT) calculations indicate a weak overlap between the VB and conduction band (CB), and the semimetallic character of the deposited Bi films was confirmed by an increase of electrical resistivity with temperature. The recorded notably higher photocurrent of Bi films under UV-visible light irradiation compared to visible light is attributed to a band-to-band transition and surface plasmonic resonance (SPR) of Bi particles. Further experimental evidence for high photocurrent density arising from the Bi films was provided by post-synthetic reductive surface treatment. Furthermore, photocatalytic measurements revealed that semimetallic Bi films generate  $\cdot\text{OH}$  radicals and promote the photocatalytic oxidation of NO at the indoor air level. Compared to conventional semiconductor photocatalysts, semimetallic Bi exhibits a more complex band structure which gives rise to a new type of photocatalytic mechanism.

## 2. Experimental Procedure

### 2.1 Synthesis

Bismuth films used in this study were obtained from an electrochemical deposition method. The deposition solution was prepared by adding  $\text{Bi}(\text{NO}_3)_3 \cdot 5\text{H}_2\text{O}$  (0.971g, Aladdin) to an acetic acid solution (2 v/v%, 1 L). Fluorine-doped tin oxide (FTO) conducting glass with 4  $\text{cm}^2$  exposed area was used as substrate. Prior to cathodic deposition, the substrates were cleaned ultrasonically in acetone, anhydrous ethanol, alkaline solution (1 M) and deionized water for 20 minutes in turn, then dried in air at 60  $^\circ\text{C}$ . The deposition process was carried out by cyclic voltammetry (CV) at room temperature. The applied potential varied from -0.64 to -0.04 V (vs. SCE), and 300 circles were programmed at 50 mV/s scan rate for typical deposition. After electrodeposition, the deposited black film was washed with deionized water and dried under ambient conditions.

### 2.2 Characterization

Powder X-ray diffraction (PXRD) analysis was conducted on a PANalytical X'pert diffractometer operated at 40 kV and 40 mA using  $\text{Cu K}_\alpha$  radiation. Scanning electron microscopy (SEM) was performed on a Hitachi S-4800 microscope. Transmission electron microscopy (TEM) images were recorded on a FEI Tecnai G2 20 microscope operated at 200 kV. X-ray photoelectron spectroscopy (XPS) measurements were conducted on a Thermo ESCALAB 250Xi with  $\text{Al K}_\alpha$  emission at 1486.6 eV. All binding energies were referenced to the C 1s peak at 284.8 eV. Diffuse reflectance spectra (DRS) data were recorded on a Shimadzu UV-2600 spectrophotometer equipped with an integrating sphere using  $\text{BaSO}_4$  as the reflectance standard sample. Absorbance values were transformed by the Kubelka-Munk method. Electron spin resonance (ESR) signals of radicals spin-trapped by 5,5-dimethyl-1-pyrroline N oxide (DMPO) were recorded at room temperature on a JES FA200 spectrometer. Samples for ESR measurement were prepared by mixing Bi films in a 50 mM DMPO solution tank and they were irradiated with a UV lamp. The electrical resistivity was measured on a temperature dependent Hall effect test system (ET9003). Thermogravimetric (TG) and differential scanning calorimetric (DSC) analysis were performed with DSC823 and TGA/SDTA85/e systems at a heating rate of 10  $^\circ\text{C}/\text{min}$  from 25

to 450  $^\circ\text{C}$  in nitrogen atmosphere. Synchrotron XRD experiments were performed at the beamline BL14B1 of Shanghai Synchrotron Radiation Facility (SSRF) at a wavelength of 1.2398  $\text{\AA}$ . A Si (111) double crystal monochromator was employed to monochromatize the beam, and the X-ray incidence angle was set to 0.2 $^\circ$  for film samples.

### 2.3 Theoretical calculations

All the calculations were performed at the generalized gradient approximation (GGA) functional of Perdew-Burke-Ernzerhof (PBE) level with the plane wave of Ultrasoft pseudopotential implemented in the CASTEP package.<sup>13</sup> Cut-off energy for the plane wave was chosen to be 400 eV, with  $5 \times 10^{-7}$  eV/atom for SCF tolerance. Monkhorst-Pack k-points were set to  $5 \times 5 \times 2$ . The electronic structures were calculated based on the fully relaxed lattice parameters and ionic positions. For the calculation of the density of states (DOS), a larger  $6 \times 6 \times 2$  k-point set was used.

### 2.4 Photoelectrochemical and photocatalytic measurements

All photoelectrochemical (PEC) measurements were conducted in a three electrode system on a CH 660D electrochemical work station, using the FTO glass with or without Bi films as the working electrode, saturated calomel electrode (SCE) as the reference electrode, and Pt wire as the counter electrode, and potentials are quoted with respect to SCE. For photoelectrochemical tests, the working electrode was irradiated from the Bi films side under a 300 W Xe lamp. Incident visible-light was obtained by utilizing a 420 nm cutoff filter. The photocurrent-time dependence of Bi films at open circuit potential (OCV) was measured in 0.5 M  $\text{Na}_2\text{SO}_4$  under chopped illumination with 40 s light on/off cycles. Photocatalytic activity was investigated by removal of NO at ppb levels in a continuous flow reactor at ambient temperature. Details of the reactor setup have been reported in previous studies.<sup>14</sup> Either a 100 W tungsten halogen lamp with a 420 nm cutoff filter or a UV lamp (280 nm) was vertically placed outside the reactor. Required pieces of Bi films ( $2 \times 2$  cm) were placed on a dish accordingly. The NO gas was acquired from a compressed gas cylinder at a concentration of 100 ppm of NO ( $\text{N}_2$  balance). The initial concentration of NO was diluted to about 550 ppb by the air stream. The desired relative humidity (RH) level of the NO flow was controlled at 50% by passing the zero air streams through a humidification chamber. The gas streams were premixed completely by a gas blender, and the flow rate was controlled at 2.4 L/min by a mass flow controller. After the adsorption-desorption equilibrium was achieved, the lamp was turned on. The concentration of NO was continuously monitored by a chemiluminescence NO analyzer (Thermo Environmental Instruments Inc., 42i-TL). The removal ratio ( $\eta$ ) of NO was calculated as  $\eta (\%) = (1 - c/c_0) \times 100\%$ , where  $C$  and  $C_0$  are concentrations of NO in the outlet stream and the feeding stream, respectively.

## 3. Results and discussion

### 3.1 Structure, morphology and surface compositions of the deposited films

Figure 1 shows the PXRD pattern of the obtained films. Except for diffraction peaks arising from the FTO substrate, no further impurities were observed, and the PXRD pattern agrees well with

reference data for pure rhombohedral Bi (space group:  $R\bar{3}m$ , JCPDS No. 44-1246) with calculated lattice constants  $a = 4.567(6)$  Å and  $b = 11.91(1)$  Å. The thermal stability of the obtained Bi films was investigated with TG/DSC analyses on Bi particles (Figure S1). The observed weight loss in the 25 - 270 °C range (3.5%) is due to surface absorbed oxygen and water, and the subsequent weight gain above the melting point of Bi (270 °C) points to the formation of BiN from Bi and N<sub>2</sub>.<sup>15</sup> Synchrotron XRD patterns of Bi films annealed at 200 °C were recorded with small incidence angle (cf. Figure S2). Comparison of room temperature data to patterns recorded at 200 °C indicate that the obtained Bi films are stable up to 200 °C and that no crystalline bismuth oxides formed during thermal treatment.

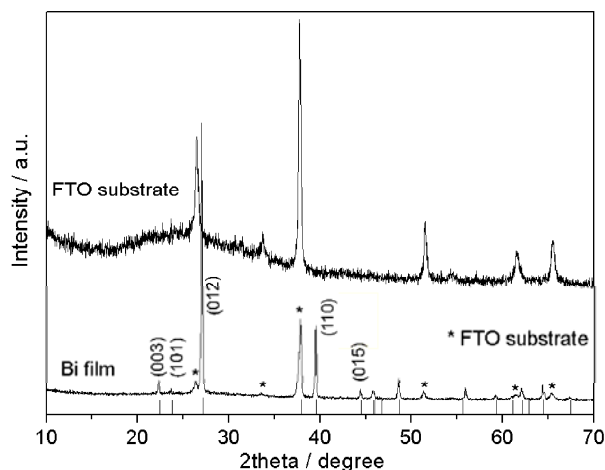


Figure 1. PXRD patterns of Bi film and FTO substrate.

The thickness of the obtained films was around 400 nm according to the cross-sectional SEM image (cf. Figure S3). Figure 2 shows the typical plane view SEM images of Bi films consisting of a compact layer with particles in the size range of several hundred nanometers. In addition, some larger particles were observed on the top of this layer. TEM provided further insight into the morphology and microstructure of the obtained particles, as shown in Figure 3. The presence of irregular particles around several hundreds of nanometers in size (cf. Figure 3a) is in line with the SEM observations. Nevertheless, TEM images recorded at higher magnification (cf. Figure S4) revealed the presence of a surface layer with a thickness of several nanometers (2-8 nm) on the particles, which may arise from the oxidation of Bi upon contact with air.<sup>16</sup> The product particles can be undoubtedly identified as elemental bismuth from their characteristic (110), (104) and (01-4) reflections in the selected area electron diffraction (SAED) pattern (inset of Figure 3b). Moreover, the observed lattice fringes with a  $d$ -spacing of 0.33 nm which are observed in the high-resolution TEM (HRTEM) image match well with the (012) crystal plane distance of bismuth. Both techniques thus indicate the single-crystalline character of the Bi particles. No other crystalline phases were observed, thereby indicating that the surface layer is amorphous.

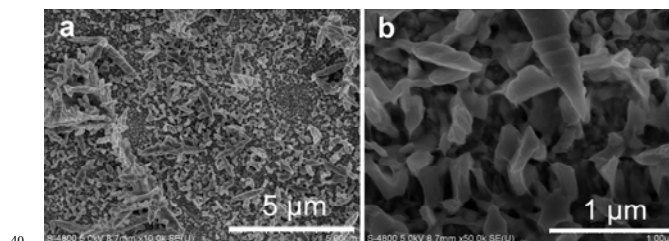


Figure 2. Typical SEM images of Bi films recorded at different magnifications.

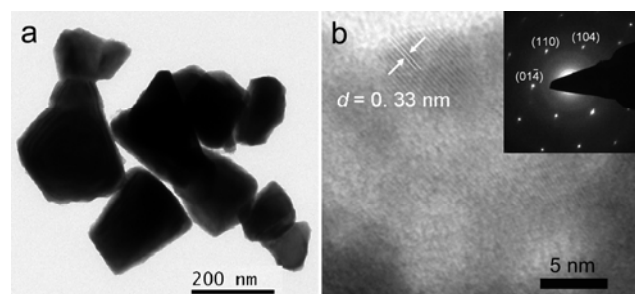
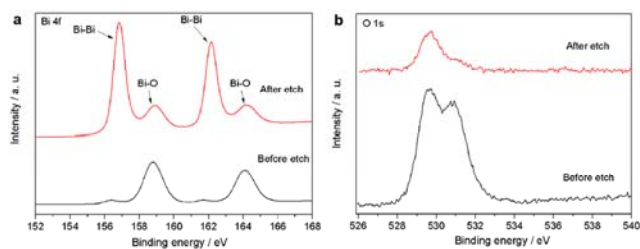


Figure 3. Representative TEM images of Bi particles.

To investigate the composition and chemical valence states of this surface layer, we compared the XPS of Bi particles before and after ion etching for 200s. XPS survey spectra (Figure S5a) indicate the presence of Bi, O and C. According to the peak ratios, the molar ratio between Bi and O prior to the etching process is around 1:3, thus pointing to an oxygen rich surface of the Bi particles. After etching for 200 s, the molar ratio of Bi:O increases sharply to 2.5:1, suggesting that the oxide layer is exclusively formed on the surface. Bi 4f XPS spectra before and after etching show considerable differences (Figure 4a). Peaks centered around 156.8 and 162.1 eV are typically attributed to the Bi-Bi bonds of elemental Bi,<sup>17</sup> while peaks at 158.9 and 164.2 eV are characteristic of Bi ions in bismuth oxides,<sup>18</sup> thereby further demonstrating that the oxide layer only exists on the surface of the elemental Bi substrate. In addition, two peaks at 529.6 and 530.8 eV for O 1s before etching were observed (Figure 4b), which arise from Bi-O with lower binding energy and the absorbed oxygen (OH<sup>-</sup> or CO<sub>3</sub><sup>2-</sup> groups) on the surface with higher energy.<sup>19</sup> The C 1s peaks at 286 and 288.1 eV further confirmed the presence of functional groups on the material surface, such as -CHO and -OH (Figure S5b),<sup>17</sup> which can play an important role in photocatalytic oxidation processes. Nevertheless, after etching for 200 s, the amount of such surface absorbed groups is remarkably reduced as shown in Figure 4b and Figure S5b. All these results indicate that the surface amorphous layer observed in TEM images (Figure S4) is composed of an oxygen rich bismuth oxide phase.



**Figure 4.** (a) Bi 4f and (b) O 1s XPS spectra of Bi particles before and after ion etching.

### 3.2 Optical properties and band structure

The as-synthesized Bi films exhibited black color (cf. inset of Figure 5) and no color change was observed over a period of half a year after deposition. To exclude the influence of FTO substrate on the optical properties, UV-vis absorption spectra of Bi powders were recorded on samples removed from the FTO substrate (Figure 5). Surprisingly, no strong absorption in the visible light range was observed. The absorption onsets were determined as 3.18, 4.40 and 4.99 eV, respectively, from the plot of the transformed Kubelka-Munk function versus the energy of light (inset of Figure 5). Moreover, a weak absorption in the visible range between 400 and 500 nm was observed which might arise from band tails or midgap states due to the surface amorphous oxide layer. Related phenomena have been previously observed for TiO<sub>2</sub><sup>2b</sup> and boron.<sup>5d</sup> Given that the optical properties of the as-synthesized Bi are much more complex in comparison with semiconductor photocatalysts, we conducted first-principles calculations of the electronic structures of elemental Bi. As the particle size and film thickness of the present samples clearly exceed the critical value for a semimetal-semiconductor transition (ca. 50 nm and below),<sup>9</sup> bulk Bi with a rhombohedral crystal structure was selected as a model. Moreover, the electrical resistivity of Bi films increased with increasing the temperature from 190 K to 300 K (cf. Figure S6), i.e. the temperature coefficient of the resistivity is positive and the material exhibits metallic properties. The calculated lattice constants ( $a = 4.613 \text{ \AA}$  and  $b = 11.374 \text{ \AA}$ ) agree well with the experimental values. Figure 6 shows the calculated band structure and DOS of bulk Bi. The Fermi level is located within the CB, and a weak overlap between the VB and CB was observed, indicating semimetallic characteristics of bulk Bi.<sup>20</sup> Both CB and VB are mainly constituted of Bi p orbitals, and the corresponding schematic band structure of semimetallic Bi is shown in Figure 7. Other than in the well-described typical semiconductors, the CB and VB of semimetallic Bi overlap, so that electrons with matching energy can occupy either band. As a consequence, the strong absorption observed in the UV range cannot be explained in terms of an electron transition from the occupied VB to the unoccupied CB. Based on our theoretical calculations, an indirect transition (2.65 eV) between the band below the VB and the VB (cf. Figure 6) could be possible under light excitation. B<sub>1</sub> and B<sub>1</sub>' depict the bands above the CB and below the VB, respectively, as

shown in Figure 7. According to this model, the observed band gap of 3.18 eV can be assigned to a B<sub>1</sub> to VB transition from an occupied level to the valence band. The calculated value (2.65 eV) is smaller than the experimental value (3.18 eV) as a result of the well known band gap underestimation within the framework of standard DFT. Furthermore, several recent studies have clearly demonstrated that Bi particles display strong SPR in the UV range (228-280 nm) depending on their particle size and shape.<sup>21</sup> The occurrence of SPR signals has been demonstrated for Bi crystals with several hundred nanometers in size, and Ma et al. specifically determined two SPR absorption peaks at 228 and 256 nm for mixed plate-like crystals (40-70 nm) and polyhedra (500 nm) of Bi.<sup>21b</sup> As two different size ranges of Bi particles were observed in the current work (Figure 2), the observed energies of 4.40 and 4.99 eV could be attributed to the respective SPR of these Bi particles. Further studies on the exact quantification of the band structure are now in progress.

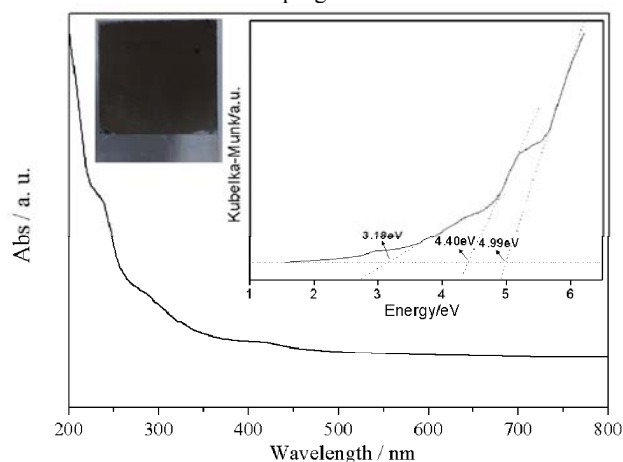


**Figure 5.** UV-vis absorption spectra of Bi powders (right inset: Kubelka-Munk transformed spectra; left inset: representative black Bi film).

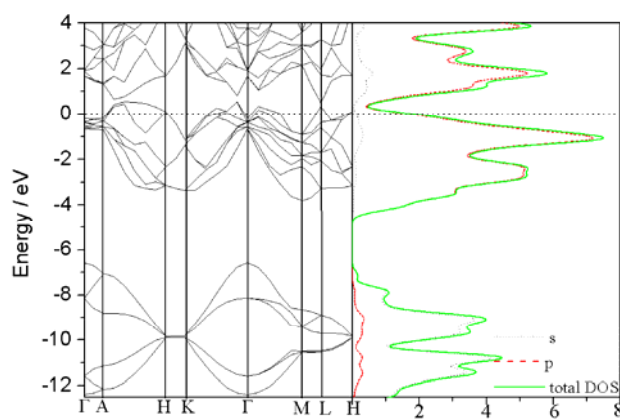


**Figure 6.** Calculated electronic band structure (left) and DOS (right) of Bi.

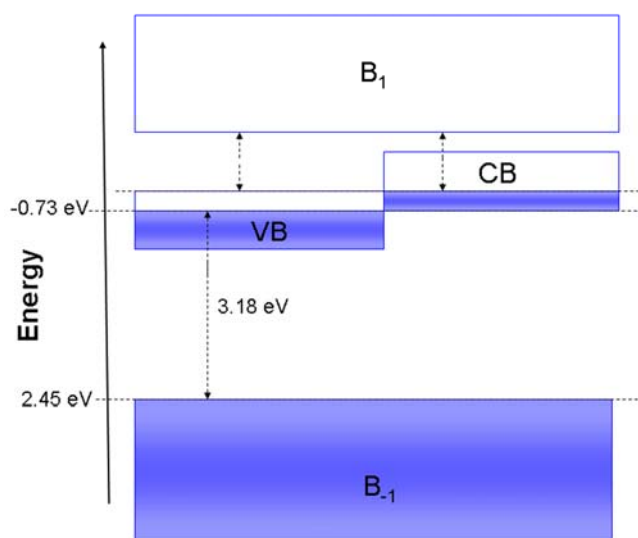


Figure 7. Schematic band structure of semimetallic Bi.

### 3.3 Photoelectrochemical properties

Figure 8a shows photocurrent-voltage curves of Bi films under both UV-visible and visible ( $\lambda > 420$  nm) light illumination, which clearly indicate that the Bi films exhibit PEC performance. The recorded photocurrent under UV-visible light irradiation is ca. 4 times higher than in the presence of visible light. This enhanced PEC performance can be ascribed to the strong UV light absorption of Bi particles (Figure 5), which results in a larger photocurrent through more efficient utilization of UV light. These results imply that electrons and holes are generated as charge carriers within black Bi particles under illumination. Furthermore, the linear-sweep voltammograms (LSVs) exhibited a related difference in PEC performance under UV-visible and visible light illumination among a wide potential bias.

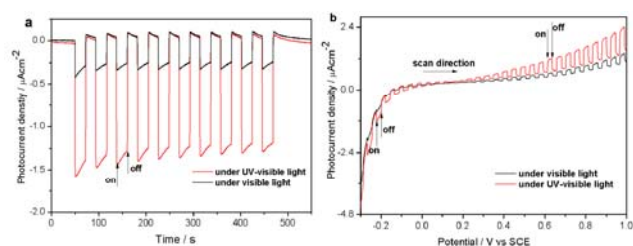


Figure 8. (a) Photocurrent-time curves at OCV under UV/vis and visible light (>420 nm) irradiation with 40 s light on/off cycles; (b) linear-sweep voltammograms under UV/vis and visible light (>420 nm) irradiation, collected with a scan rate of  $1 \text{ mV s}^{-1}$ .

As the obtained Bi films were covered by an amorphous oxide layer with a thickness in the range of 2-8 nm, elucidation of its influence on the photoelectrochemical properties of elemental Bi is essential. Given that the melting point of Bi is as low as  $270^\circ\text{C}$  (Figure S1), removal of the surface amorphous layer by etching

with  $\text{H}_2$  at low temperature is difficult. Therefore, an electrochemical reduction process is performed on films after photocurrent measurements, and the detailed reduction process is monitored in Figure S7. After reduction, the OCV of the Bi electrode became far more negative than the value prior to reduction ( $-0.13 \text{ V}$ ) and it remained stable at  $-0.25 \text{ V}$  (Figure 9a), while the Bi electrode resistance decreased sharply according to electrochemistry impedance spectroscopy (EIS) data shown in Figure S8. All in all, these results clearly demonstrate that the Bi electrode surface has been reduced, i.e. the surface amorphous oxide layer was removed. Furthermore, the corresponding PEC performances of the Bi electrode were studied under chopped UV-vis light. The photocurrent density was notably enhanced after electrochemical reduction (Figure 9b), and the 4.4-fold increase compared to the pristine material indicates that the amorphous oxide layer on the electrode surface impaired its PEC performance. Moreover, the observed photo-response arises from semimetallic Bi itself instead of the surface amorphous layer. On the other hand, the recombination effects of photogenerated electrons and holes after reduction became more prominent compared to the electrode photocurrent behavior before reduction, according to the initial instantaneous photocurrent under irradiation (Figure 9b), thereby indicating that the amorphous oxide layer may be beneficial for the separation of photogenerated carriers. Very recently, Chen et al. demonstrated that the application of a 1 nm thick disordered layer onto  $\text{TiO}_2$  nanocrystals can provide trapping sites for photogenerated carriers and prevent them from rapid recombination.<sup>2b</sup> In contrast, Liu et al. observed that such surface amorphous layers impair the photocatalytic activity of elemental boron remarkably.<sup>5d</sup> These contradictory observations are probably due to the different thicknesses of the respective surface amorphous layers. In the current work, a 2 - 8.5 nm surface amorphous layer was observed (Figure S4), which is sufficiently wide to trap the photogenerated carriers, thereby decreasing the amounts of photoexcited charge carriers migrating to the surface. Therefore, the PEC performance of semimetallic Bi under UV/vis light is improved by a factor of 4.4 after electrochemical reduction of the surface amorphous oxide layer.

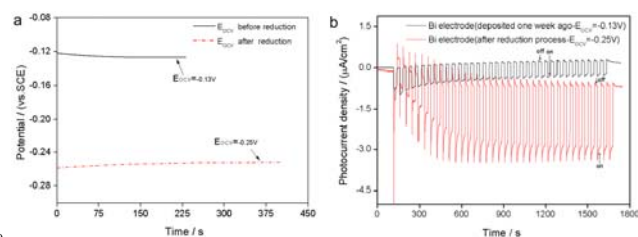


Figure 9. (a) Open circuit voltage for the Bi electrode before and after electrochemical reduction in  $0.5 \text{ M Na}_2\text{SO}_4$  solution; (b) photocurrent-time curve for the above Bi electrode before and after reduction at OCV under UV/vis irradiation.

### 3.4 Photocatalytic oxidation of NO

Although the PEC performance of semimetallic Bi can be

enhanced after electrochemical reduction, Bi is easily oxidized upon contact with air. Hence, it is almost impossible to exclude the formation of a surface amorphous layer for photocatalytic applications. The photocatalytic activity of black Bi films was evaluated for the photooxidation of NO at the indoor air level. Figure S9 shows the variation of NO concentration ( $c/c_0$  %) with irradiation time over the Bi films ( $20 \text{ cm}^2$ ) under UV and visible light ( $> 420 \text{ nm}$ ) irradiation. Here,  $c_0$  is the initial concentration of NO and  $c$  is the concentration of NO after a given photocatalytic reaction for time interval  $t$ , respectively. The photodegradation of NO under visible light irradiation is negligible. However, under UV light irradiation, the NO concentration decreased rapidly through photocatalytic oxidation within 7 min. After 20 min of irradiation, the removal ratio of NO for Bi films is 23.8%. Formation of  $\text{NO}_2$  instead of  $\text{NO}_3^-$  as the main oxidation product points to photocatalytic oxidation of NO to  $\text{NO}_2$  as the major process. The removal ratio of NO can be further raised to 37.7% through increasing the area of Bi films to  $80 \text{ cm}^2$  as shown in Figure 10. It is noteworthy that the black Bi films did not reveal any reduction of their photocatalytic activity under UV light irradiation after five cycles (Figure 10). Moreover, XRD and SEM (Figure S10 and Figure S11) investigations of the Bi films after photocatalytic tests showed that they did not undergo significant structural and morphological changes, which suggests promising stability for further applications. As photogenerated reactive radicals play a key role in the oxidation of NO, we examined the formation of reactive radicals through ESR spectra of Bi films under UV light, using the most sensitive method to detect radicals.<sup>22</sup> Figure S12 compares the DMPO spin-trapping ESR spectra of Bi films in the dark and under UV light irradiation. Whereas no signal was observed in the dark, four characteristic peaks of DMPO- $\cdot\text{OH}$  adducts with an intensity ratio of 1:2:2:1 were present under UV light irradiation,<sup>23</sup> indicating the production of  $\cdot\text{OH}$  radicals in the irradiated Bi films. Hence, the free  $\cdot\text{OH}$  radicals could be the main active oxygen species in the photocatalytic oxidation of NO to  $\text{NO}_2$ .

The above results clearly demonstrate the photocatalytic activity of semimetallic Bi. The working mechanism of conventional semiconductors is based on the generation of electron-hole pairs for photocatalytic reactions via light-driven electron transitions from the occupied VB to unoccupied CB states. However, the incident light excitation process is more complex for semimetallic Bi due to the overlap of CB and VB. Depending on the excitation energy, transitions can be assigned to either  $B_{-1}$  to VB, or VB to  $B_1$ , or to a combination of both scenarios (Figure 7). Visible ( $\lambda > 420 \text{ nm}$ ) light irradiation is not sufficient to excite the  $B_{-1}$  to VB (3.18 eV) transition of semimetallic Bi. Therefore, the recorded photocurrent of Bi films under UV-visible light irradiation is ca. 4-fold higher than for visible light. Furthermore, theoretical calculations suggest that the transition from VB to  $B_1$  already sets in at rather low energies (Figure 6). Under UV-visible light irradiation, the transition both from  $B_{-1}$  to VB and VB to  $B_1$  could thus be excited and electrons with sufficient energy can occupy either band of the overlapping CB and VB. Hence, the VB could provide trapping sites for photogenerated carriers and prevent them from rapid recombination. The combination of long electron mean free path and small effective mass in Bi facilitates the movement of

photoinduced carriers to the surface of particles.<sup>24</sup> Nevertheless, it is surprising that the visible light driven photooxidation performance of semimetallic Bi of NO is negligible, although the films exhibit PEC performance under visible light irradiation (Figure S9). As the CB and VB of Bi are overlapping, the  $B_{-1}$  maximum of Bi was determined to be 1.81 eV (Figure S13), which is 0.19 eV smaller than that of anatase  $\text{TiO}_2$ .<sup>25</sup> The VB maximum of anatase  $\text{TiO}_2$  is located at + 2.64 V vs NHE at pH 7.<sup>26</sup> Hence, the redox potential for the  $B_{-1}$  maximum of Bi (+ 2.45 eV) is large enough to oxidize  $\text{OH}^-$  to  $\cdot\text{OH}$  (+ 1.9 V vs NHE), so that photodegradation of NO over Bi films under UV light irradiation was observed. Under visible light irradiation, photogenerated carriers emerge from the VB to  $B_1$  transition, but their redox potential is not sufficiently positive for the oxidation of NO. Nevertheless, the photocatalytic mechanisms of materials with metallic behavior are far less understood than those of semiconductor photocatalysts. For example, Irvine et al. pointed out that metallic photocatalysts exhibit intermediate mechanisms compared to photoelectrocatalysts and photocatalysts.<sup>7</sup> In summary, Bi films have an innovative and promising potential as photocatalysts, and further optimization studies via surface modification and catalyst coupling strategies are now under way.

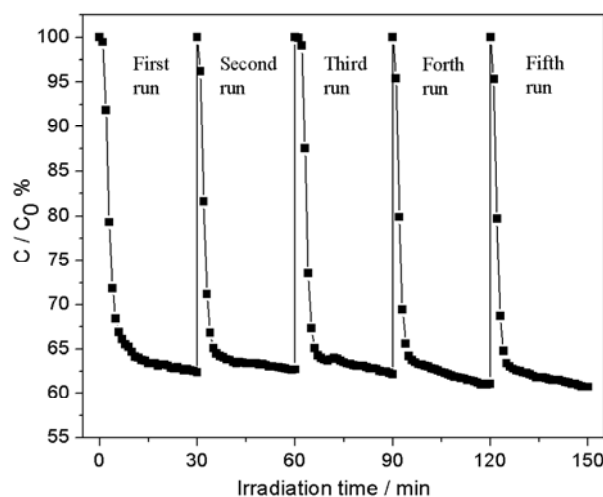


Figure 10. Cycling runs of photocatalytic activities of Bi films under UV light irradiation for removal of NO in air.

#### 4. Conclusions

Semimetallic Bi is introduced as a new material type for the photocatalytic oxidation of NO in air. The deposited Bi films are capable of generating electrons and holes under UV and visible light irradiation, and detection of  $\cdot\text{OH}$  radicals in combination with photoconductivity measurements provides clear evidence for this key property. In contrast to most semiconductor photocatalysts, Bi films exhibited metallic properties, and their strong UV absorption arises from a band-to-band transition and SPR of Bi particles. The amorphous oxide layer on the Bi surface impairs the PEC performance of semimetallic Bi. After

electrochemical reduction of the surface amorphous layer, the photocurrent density of Bi was enhanced by a factor of 4.4, indicating clearly the generation of photogenerated carriers from semimetallic Bi without participation of residual surface layer parts. These results open up new avenues for exploration of elemental photocatalysts and for the targeted development of semimetallic photocatalysts as a new alternative to classic semiconductor materials.

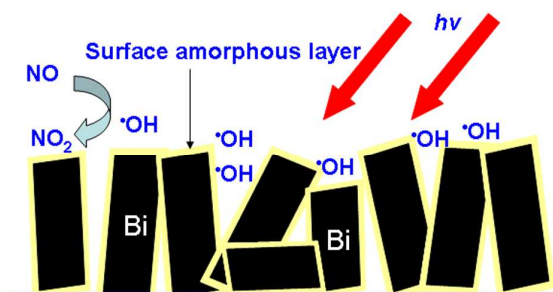
## Acknowledgements

This work was supported by the National Natural Science Foundation of China (51102245), Sichuan Youth Science and Technology Foundation (2013JQ0034), the Innovative Research Team of Sichuan Provincial Education Department and SWPU (2012XJZT002, 2012XJZ016). We thank SSRF for beamtime at beamline BL14B1. G. R. P. acknowledges financial support by the Swiss National Science Foundation (SNSF Professorship PP00P2-13348/1) and by the University of Zurich.

## Notes and references

- <sup>a</sup> State Key Laboratory of Oil and Gas Reservoir and Exploitation, Southwest Petroleum University, Chengdu 610500, china. Fax: + 86 28 83037406; Tel: +86 28 83037409; E-mail: yzhou@swpu.edu.cn
- <sup>b</sup> School of Materials Science and Engineering, Southwest Petroleum University, Chengdu 610500, china.
- <sup>c</sup> College of Environmental and Biological Engineering, Chongqing Technology and Business University, Chongqing 400067, China.
- <sup>d</sup> Department of Chemistry, University of Zurich, CH-8057 Zurich, Switzerland.
- † Electronic Supplementary Information (ESI) available: [TG/DSC curves of the as-synthesized Bi films, synchrotron XRD patterns of as-deposited and annealed (200 °C) Bi films, cross-sectional SEM image, TEM image, representative survey and C 1s XPS spectra of Bi particles before and after ion etching, temperature dependence of the electrical resistivity, current-time curve for Bi reduction, EIS for the Bi electrode before and after electrochemical reduction, photocatalytic activity of Bi films under UV and visible light irradiation, time-dependent of DMPO-<sup>•</sup>OH ESR spectra, PXRD pattern and SEM of Bi films after photocatalytic tests, XPS valence band spectrum of Bi films.]. See DOI: 10.1039/b000000x/
- (a) A. Kudo, Y. Miseki, *Chem. Soc. Rev.*, 2009, **38**, 253; (b) X. B. Chen, S. H. Shen, L. J. Guo, S. S. Mao, *Chem. Rev.*, 2010, **110**, 6503; (c) H. Tong, S. Ouyang, Y. P. Bi, N. Umezawa, M. Oshikiri, J. H. Ye, *Adv. Mater.*, 2012, **24**, 229.
  - (a) G. Liu, L. Z. Wang, H. G. Yang, H. M. Cheng, G. Q. Lu, *J. Mater. Chem.*, 2010, **20**, 831. (b) X. B. Chen, L. Liu, P. Y. Yu, Mao, S. S. *Science*, 2011, **331**, 746;
  - (a) Z. G. Yi, J. H. Ye, N. Kikugawa, T. Kako, S. Ouyang, H. Stuart-Williams, H. Yang, J. Y. Cao, W. J. Luo, Z. S. Li, Y. Liu, R. L. Withers, *Nature Mater.*, 2010, **9**, 559; (b) G. Wang, B. B. Huang, X. C. Ma, Z. Y. Wang, X. Y. Qin, X. Y. Zhang, Y. Dai, M.-H. Whangbo, *Angew. Chem. Int. Ed.*, 2013, **52**, 4810.
  - X. C. Wang, K. Maeda, A. Thomas, K. Takanabe, G. Xin, J. M. Carlsson, K. Domen, M. Antonietti, *Nature Mater.*, 2009, **8**, 76.
  - (a) Z. H. Kang, C. H. A. Tsang, N. B. Wong, Z. D. Zhang, S. T. Lee, *J. Am. Chem. Soc.*, 2007, **129**, 12090. (b) F. Wang, W. K. H. Ng, J. C. Yu, H. J. Zhu, C. H. Li, L. Zhang, Z. F. Liu, Q. Li, *Appl. Catal. B*, 2012, **111-112**, 409. (c) G. Liu, P. Niu, L. C. Yin, H. M. Cheng, *J. Am. Chem. Soc.*, 2012, **131**, 9070. (d) G. Liu, L. C. Yin, P. Niu, W. Jiao, H. M. Cheng, *Angew. Chem. Int. Ed.*, 2013, **52**, 6242.
  - G. Liu, P. Niu, H. M. Cheng, *ChemPhysChem.*, 2013, **14**, 885.
  - X. X. Xu, C. Randorn, P. Efstathiou, J. T. S. Irvine, *Nature Mater.*, 2012, **11**, 5958.

- (a) F. Y. Yang, K. Liu, K. Hong, D. H. Reich, P. C. Searson, C. L. Chien, *Science*, 1999, **284**, 1335. (b) B. O'Brien, M. Plaza, L. Y. Zhu, L. Perez, C. L. Chien, P. C. Searson, *J. Phys. Chem. C*, 2008, **112**, 12018. (c) J. P. Michenaud, J. P. Issi, *J. Phys. D*, 1972, **5**, 3061.
- (a) L. Li, Y. W. Yang, X. H. Huang, G. H. Li, R. L. Ang, D. Zhang, *Appl. Phys. Lett.*, 2006, **88**, 103119. (b) K. Liu, C. L. Chien, P. C. Searson, *Appl. Phys. Lett.*, 1998, **58**, 14681.
- (a) J. L. Costa-Kramer, N. Garcia, H. Olin, *Phys. Rev. Lett.*, 1997, **78**, 4990. (b) M. R. Black, Y. M. Lin, S. B. Cronin, O. Rabin, M. S. Dresselhaus, *Phys. Rev. B*, 1997, **78**, 4990.
- (a) Y. Zhou, K. Vuille, A. Heel, B. Probst, R. Kontic, G. R. Patzke, *Appl. Catal. A*, 2010, **375**, 140. (b) Y. Zhou, F. Krumeich, A. Heel, G. R. Patzke, *Dalton Trans.*, 2010, **39**, 6043. (c) M. Ge, Y. F. Li, L. Liu, Z. Zhou, W. Chen, *J. Phys. Chem. C*, 2011, **115**, 5220. (d) M. Ge, L. Liu, W. Chen, Z. Zhou, *CrystEngComm*, 2012, **14**, 1038.
- D. C. Ma, J. Z. Zhao, Y. Zhao, X. L. Hao, Y. Lu, *Chem. Eng. J.* 2012, **209**, 273.
- S. J. Clark, M. D. Segall, C. J. Pickard, P. J. Hasnip, M. I. J. Probert, K. Refson, M. C. Payne, *Z. Kristallogr.*, 2005, **220**, 567.
- W. D. Zhang, Q. Zhang, F. Dong, *Ind. Eng. Chem. Res.*, 2013, **52**, 6740.
- R. L. Fu, S. Xu, Y.-N. Lu, J.-J. Zhu, *Cryst. Growth Des.*, 2005, **5**, 1379.
- S. C. Warren, A. C. Jackson, Z. D. Cater-Cyker, F. J. DiSalvo, U. Wiesner, *J. Am. Chem. Soc.*, 2007, **129**, 10072.
- (a) W. E. Morgan, W. J. Stec, J. R. Van Vazer, *Inorg. Chem.*, 1973, **12**, 953. (b) X. W. Liu, H. Q. Cao, J. F. Yin, *Nano Res.*, 2011, **4**, 470.
- (a) F. Dong, S. C. Lee, Z. B. Wu, Y. Huang, M. Fu, W.-K. Ho, S. C. Zou, B. Wang, *J. Hazard. Mater.*, 2011, **195**, 346. (b) R. H. Li, W. X. Chen, H. Kobayashi, C. X. Ma, *Green Chem.*, 2010, **12**, 212.
- H. F. Cheng, B. B. Huang, J. B. Lu, Z. Y. Wang, B. Xu, X. Y. Qin, X. Y. Zhang, Y. Dai, *Phys. Chem. Chem. Phys.*, 2010, **12**, 15468.
- J. S. Qi, D. Shi, J. J. Zhao, X. F. Jiang, *J. Phys. Chem. C*, 2008, **112**, 10745.
- (a) Y. W. Wang, B. H. H. Hong, K. S. Kim, *J. Phys. Chem. B*, 2005, **109**, 7067. (b) D. C. Ma, J. Z. Zhao, R. Chu, S. S. Yang, Y. Zhao, X. L. Hao, L. Z. Li, L. Zhang, Y. Lu, C. Z. Yu, *Adv. Powder Tech.*, 2013, **24**, 79. (c) D. Velasco-Arias, I. Zumeta-Dubé, D. Díaz, P. Santiago-Jacinto, V. Ruiz-Ruiz, S. Castillo-Blum, L. Rendón, *J. Phys. Chem. C*, 2012, **116**, 14717.
- K. Zhao, L. Z. Zhang, J. J. Wang, Q. X. Li, W. W. He, J. J. Yin, *J. Am. Chem. Soc.*, 2013, **135**, 15750.
- H. B. Fu, C. S. Pan, W. Q. Yao, Y. F. Zhu, *J. Phys. Chem. B*, 2005, **109**, 22432.
- (a) K. R. Lai, W. Wei, Y. T. Zhu, M. Guo, Y. Dai, B. B. Huang, *J. Solid State Chem.*, 2012, **187**, 103. (b) X. C. Ma, Y. Dai, M. Guo, B. B. Huang, *ChemPhysChem*, 2012, **13**, 2304.
- G. Liu, L. Z. Wang, C. H. Sun, X. X. Yan, X. W. Wang, Z. G. Chen, S. C. Smith, H. M. Cheng, G. Q. Lu, *Chem. Mater.*, 2009, **21**, 1266.
- S. Sakthivel, H. Kisch, *ChemPhysChem.*, 2003, **4**, 487.



Black semimetallic Bi films were found to be active in the photocatalytic oxidation of NO at the indoor air level.